

# SharpRazor: Automatic removal of hair and ruler marks from dermoscopy images

Reda Kasmi<sup>1</sup> | Jason Hagerty<sup>2</sup> | Reagan Young<sup>3</sup> | Norsang Lama<sup>3</sup> | Januka Nepal<sup>3</sup> | Jessica Miinch<sup>3</sup> | William Stoecker<sup>2</sup> | R Joe Stanley<sup>3</sup>

<sup>1</sup>Faculty of Technology, Laboratoire de Technologie Industrielle et de l'Information (LTII), University of Bejaia, Bejaia, Algeria

<sup>2</sup>S&A Technology, Rolla, Missouri, USA

<sup>3</sup>Department of Electrical and Computer Engineering, Missouri University of Science and Technology, Rolla, Missouri, USA

## Correspondence

Jason Hagerty, S&A Technology, Rolla, MO, 65401, USA. Email: [jrh55c@umsystem.edu](mailto:jrh55c@umsystem.edu)

## Abstract

**Background:** The removal of hair and ruler marks is critical in handcrafted image analysis of dermoscopic skin lesions. No other dermoscopic artifacts cause more problems in segmentation and structure detection.

**Purpose:** The aim of the work is to detect both white and black hair, artifacts and finally inpaint correctly the image.

**Method:** We introduce a new algorithm: SharpRazor, to detect hair and ruler marks and remove them from the image. Our multiple-filter approach detects hairs of varying widths within varying backgrounds, while avoiding detection of vessels and bubbles. The proposed algorithm utilizes grayscale plane modification, hair enhancement, segmentation using tri-directional gradients, and multiple filters for hair of varying widths. We develop an alternate entropy-based processing adaptive thresholding method. White or light-colored hair, and ruler marks are detected separately and added to the final hair mask. A classifier removes noise objects. Finally, a new technique of inpainting is presented, and this is utilized to remove the detected object from the lesion image.

**Results:** The proposed algorithm is tested on two datasets, and compares with seven existing methods measuring accuracy, precision, recall, dice, and Jaccard scores. SharpRazor is shown to outperform existing methods.

**Conclusion:** The SharpRazor techniques show the promise to reach the purpose of removing and inpaint both dark and white hair in a wide variety of lesions.

## KEYWORDS

dermoscopy, hair removal, inpainting, image processing, mathematical morphology, segmentation

## 1 | INTRODUCTION

In recent years, the incidence of skin cancer has been rising, contributing significantly to the rise in health care costs.<sup>1,2</sup> In 2021, the United States is estimated to have 115 320 new cases and 11 540 deaths attributed to skin cancer (excluding basal and squamous cell carcinoma);<sup>1</sup> a similar burden exists globally.<sup>3</sup> Nonmelanoma skin

cancer, the most common type of cancer, is increasing in parallel with melanoma.<sup>2</sup> Skin cancer is often curable when detected and treated early, yet dermatologists, even with the aid of dermoscopy, can misdiagnose these cancers.<sup>4–7</sup>

Deep learning accuracy for diagnosing dermoscopic images now exceeds that of dermatologists for both melanoma detection and exact-class diagnosis of various lesions.<sup>4–7</sup> Handcrafted techniques can

This is an open access article under the terms of the [Creative Commons Attribution-NonCommercial-NoDerivs](#) License, which permits use and distribution in any medium, provided the original work is properly cited, the use is non-commercial and no modifications or adaptations are made.

© 2023 The Authors. *Skin Research and Technology* published by John Wiley & Sons Ltd.

improve deep learning results.<sup>8</sup> Because hair artifacts can interfere with handcrafted feature recognition, hair removal has become the leading topic of artifact removal.<sup>9</sup> Shaving the hair from the lesion area is an alternate solution, but challenges such as the location of the lesion and the possibility of shaving irritation make this solution impractical.<sup>10</sup>

Numerous hair removal algorithms have been proposed using dermoscopy images. Abbas et al.<sup>11</sup> summarized the current state of hair detection and restoration. The presented survey of published methods is further evaluated in our study using traditional metrics. As Lee et al. stated,<sup>12</sup> we may group hair removal algorithms into three categories: those using mathematical morphology methods, edge detection methods, and matched filtering methods.

Lee et al.<sup>12</sup> use the top-hat transform and modified second-order Gaussian filter to enhance hair. The initial hair mask is then generated using an adaptive threshold and further refined using a k-nearest neighbor classifier. Xie et al.<sup>13</sup> proposed an algorithm that focuses on dark hair. The method is also based on the top-hat operator and an automatic threshold; the image hair area detected is reconstructed using a partial differential equation-based inpainting technique. Abbas et al.<sup>14</sup> presented a hair removal algorithm based on the first derivative of Gaussian to detect potential light and dark hairs, followed by adaptive thresholding and refinement filtering. Hair objects were inpainted using a fast marching technique.<sup>15</sup> Nguyen et al.<sup>16</sup> detected both dark and light hair using a universal matched filtering kernel. A binary hair mask was generated by local entropy thresholding and subsequently refined.

Lee et al.<sup>17</sup> proposed DullRazor, consisting of three main steps. First, hair is segmented based on the morphological closing operation. Next, the detected hair segments were inpainted using a bilinear interpolation. Finally, the hair mask is smoothed. Fiorese et al.<sup>10</sup> proposed the VirtualShave algorithm to find hair. VirtualShave used a top-hat filter with long structuring elements, followed by morphological postprocessing, finally inpainting the detected hair area with a PDE-based technique. Koehoorn et al.<sup>18</sup> used a threshold-set model, a gap-detection algorithm, morphological analysis, and further postprocessing using a skeletonizing method. Toossi et al.<sup>19</sup> detect hair using an adaptive Canny edge detector followed by image refinement by morphological operators and reconstructed using a multiresolution coherence transport inpainting. Kiani et al.<sup>20</sup> proposed E-Shaver, using the Radon transform to find hair orientation and Prewitt filters to detect hair edges. Then, a chain of filters is used to remove nonhair objects. Fleming et al.<sup>21</sup> detect all line segments in the image using Steger's line detection algorithm,<sup>22</sup> then hair segments are classified by linear discriminant analysis. Abuzaghlah et al.<sup>23</sup> segment hair by a set of directional Gaussian filters. Hair pixels are replaced by eight-directional inpainting. Huang et al.<sup>24</sup> aimed to detect thin hairs and hairs in the shade; the method emphasizes hairs by the matched filtering technique using a Gaussian-like profile. Zhou et al.<sup>25</sup> present a hair detection and removal algorithm based on line detection and curve fitting using Steger's algorithm<sup>22</sup> and the least square method.<sup>26</sup> Finally, the exemplar-based inpainting is performed.

This paper proposes a technique to detect and remove hair. It consists of seven main steps: (1) The red color plane image is transformed by smoothing and linear scaling. (2) Hair images are enhanced by two directional filters. (3) Gradients in three directions are used to detect maximum hair edges. (4) The image is binarized using an adaptive threshold. (5) White or light-colored hairs and ruler marks, overlooked in other studies, are detected and combined with the hair mask. (6) Finally, a random forest classifier identifies and removes non-hair objects. (7) Using the hair mask as a guide, a novel inpainting method is performed to remove the detected regions for the original image.

Previous hair removal algorithms were evaluated on small image sets, and many ignored light hair and ruler marks. The proposed algorithm was trained on 520 images from NIH study R43 CA153927-01 and CA101639-02A2 with manually drawn masks that indicate the presence of hair, white light-colored hairs and, rule marks. The post-processing algorithm was trained on 707 images from the same study. SharpRazor was evaluated against 7 other published methods on a set of 25 images.

## 1.1 | Preprocessing and image transformation

Each dermoscopic image is represented as an RGB image. Using the red grayscale channel ( $I_{red}$ ), a median filter with a kernel size of  $3 \times 3$  smoothes the image and reduces noisy objects such as bubbles. The resultant image was then linearly scaled by an empirically derived value of 1.64 (Figure 1).

$$I_{red}^{new} = 1.64 I_{red} \quad (1)$$

## 1.2 | Initial hair detection

Region of interest (ROI) masks are used to aid in horizontal and vertical filters by dynamically estimating hair background color. The horizontal filter for vertical hair detection (Figure 2A) consists of three in-line horizontally oriented  $5 \times 7$  mask panels (Figure 2B). The vertical filter (Figure 2C) for horizontal hair detection consists of the transposed mask panels used for vertical hair detection.

## 1.3 | Horizontal filter

The horizontal filter is guided by an ROI of  $1 \times 7$  pixels horizontally oriented. The filter segment scans the  $I_{red}^{new}$  image along each line. The presence of a probable hair pixel is determined when the range of pixel intensities covered by the filter exceeds a value of 10. The hair pixel is located at the position within the filter with the lowest value. Figure 2A illustrates how a hair pixel is located using the horizontal filter (sizes are exaggerated).

The trio of  $5 \times 7$  horizontal masks, Figure 2B, is then centered on the detected hair pixel. The central mask panel is replaced by the average of the two medians computed from the outer mask panels if

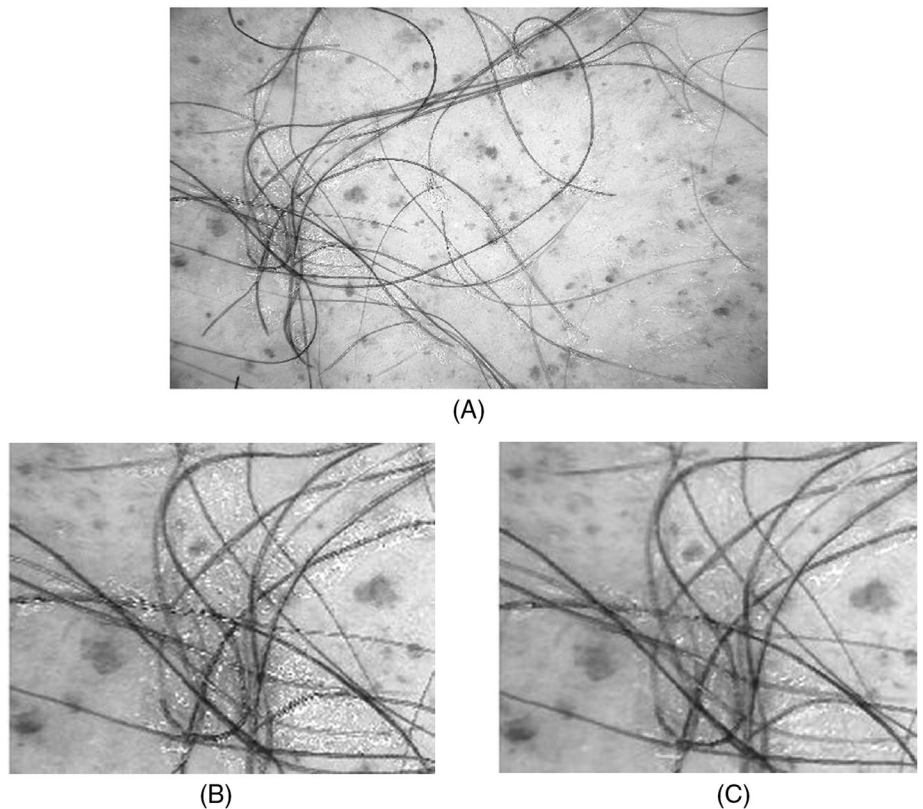


**FIGURE 1** Transformation of the red channel. The lesion (A) is the reference for zoomed in images (B) and (C). (B) Original red plane ( $I_{red}$ ), (C) scaled red channel ( $I_{red}^{new}$ ) using Equation 1.

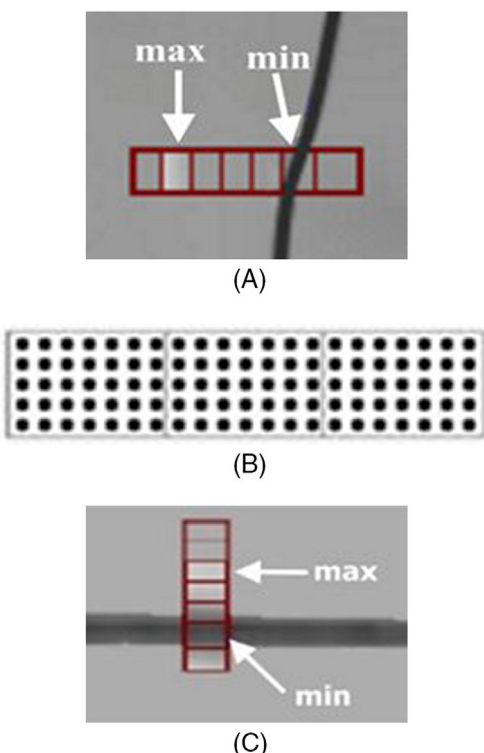


**FIGURE 2** (A) Vertical filtering, (B) vertical mask, and (C) horizontal filter.

two conditions are satisfied: the average of pixels under the central mask is lower than the two averages of the pixels under the outer mask panels; and, the average of pixels under the central mask for the blue grayscale plane is less than 180. Results of the described horizontal filtering are shown in Figure 3B.

#### 1.4 | Vertical filter

The vertical filter is guided by an ROI of  $1 \times 7$  pixels oriented vertically. The filter segment scans the grayscale image along each column. The hair pixel is found when the range of pixel intensities covered by the filter exceeds 10. The lowest pixel value locates the hair, as shown in Figure 2C. Then, like with that of the horizontal filtering procedure, the transposed horizontal filter panel (Figure 2B) is centered on the detected hair pixel. The central panel pixels are replaced by the average of the two medians computed from adjacent mask panels. Examples of vertical filter results are shown in Figure 3B.

The hair's background value is calculated to be the maximum of the vertical and the horizontal filter plane results. The background is smoothed using a morphological closing operation with a disk structuring element, radius 2.

$$\text{background} = \text{MAX}(\text{Vertical filter result}, \text{Horizontal filter result}) \quad (2)$$

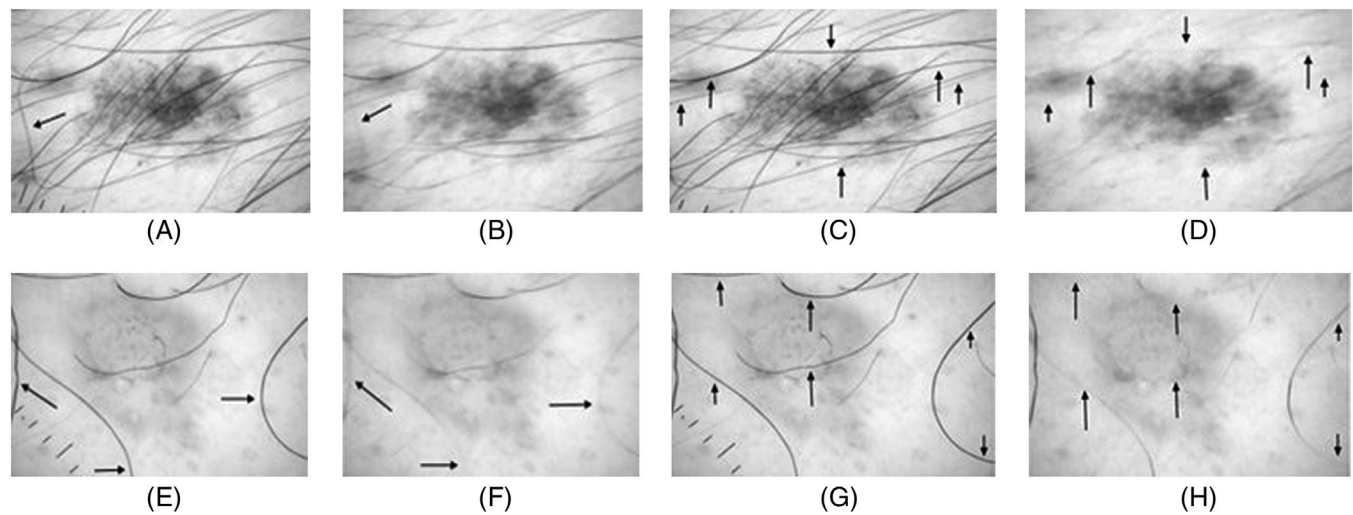


**FIGURE 3** Vertical filtering, (A and C) original image. (B and D) Horizontal filter result. Horizontal filtering, (E and G) original image. (F and H) Horizontal filter result. Arrows mark examples of primarily horizontal or vertically oriented hair segments.

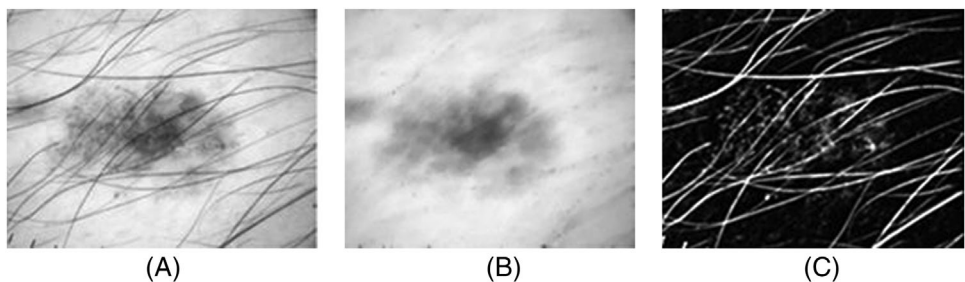


**FIGURE 4** Hair enhancement: (A) original grayscale image, (B) the estimated background, and (C) enhanced hair.

## 2 | HAIR ENHANCEMENT

Hair is enhanced by extracting the  $I_{\text{new}}$  grayscale image from the estimated background (Equation 3). Figure 4 shows an example of hair enhancement.

$$\text{Enhanced hair} = \text{Background} - I_{\text{new}} \quad (3)$$

## 3 | HAIR SEGMENTATION

Hair segmentation using gradient-based edge detection is performed. To detect hair edges, we apply the gradient in three orientations (0, 22.5, and 67.5). For each orientation, the two gradient components ( $x, y$ ) are binarized by an optimized threshold,<sup>27</sup>

$$T = 1 + \text{Otsu\_threshold} \quad (4)$$

$T$  is calculated from the gradients. Figure 5 shows the different steps performed. Finally, the hair mask is refined using two filters (Figure 6).

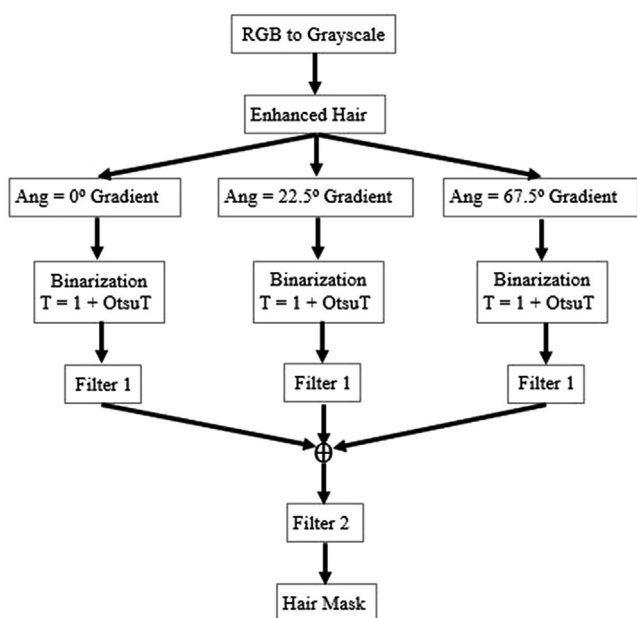


**FIGURE 5** Gradient and binarization steps to find the hair mask.

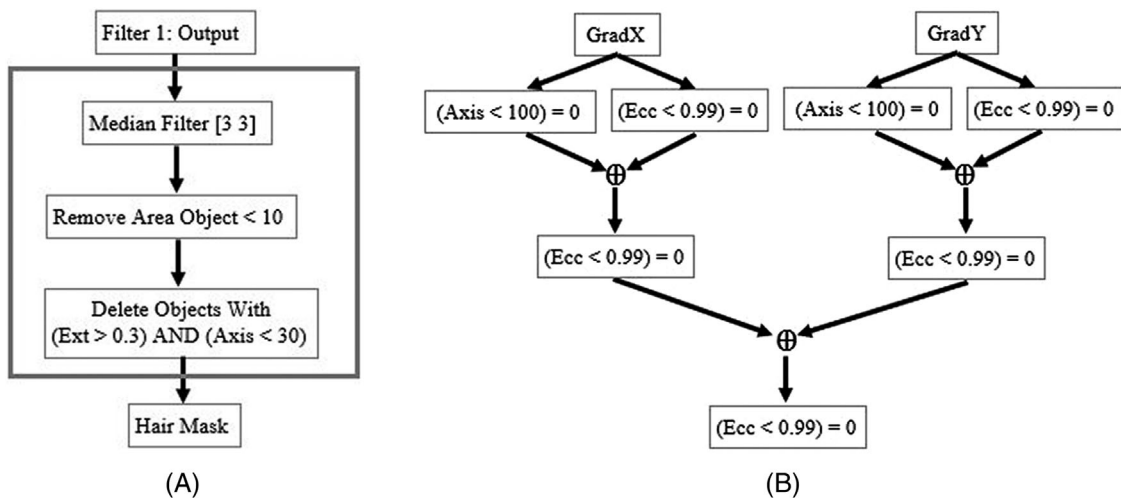


**FIGURE 6** Filters used for hair mask refinement. (A) Filter 1. (B) Filter 2.

#### 4 | RULER MARK DETECTION

Ruler marks may cause similar problems as hair in automatic analysis. First, morphological closing operation with a rectangle-structuring element  $2 \times 50$  is performed on the red plane ( $I_r$ ), a new plane is computed as (Equations 5–7):

$$I_{\text{new}} = I_{\text{rc}} - I_r \quad (5)$$

$I_{\text{new}}$ : is binarized using a threshold  $T_r$

$I_{\text{rc}}$ : result of closing operation.

$I_r$ : red plane.

$$T_r = 2/5 (\text{MAX}(I_{\text{new}}) - \text{MIN}(I_{\text{new}})) + \text{MIN}(I_{\text{new}}) \quad (6)$$

$$I_b = \begin{cases} 1 & I_{\text{new}}(x, y) > T_r \\ 0 & \text{otherwise} \end{cases}; \text{ subject to } \text{MIN}(I_{\text{new}}) \neq 0 \quad (7)$$

Nonruler marks in the binary image  $I_b$  are removed by two filters, where:

**Filter 3:** All objects less than 25 pixels length or solidity less than 0.6 are removed. Solidity is the area of the object divided by the convex hull area of the object.

**Filter 4:** Removes all objects located within the central quadrant when the image is divided into nine equal quadrants.

The resultant mask is created by a logical OR operation between the hair mask and ruler marks (Figure 7).

#### 5 | WHITE HAIR DETECTION

First, the  $I_{gm}$  plane is found by using a  $3 \times 3$  median filter applied to the blue plane B. Then, the white hair (WH) is enhanced by extracting

the  $I_{gm}$  image from the B plane (Equation 8). The WH is segmented by thresholding the enhanced WH with a threshold equal to 1.

$$\text{WH} = B - I_{gm} \quad (8)$$

To filter noise on the binarized WH mask, all objects with maximum axis less than 20 or eccentricity less than 0.90 or the ratio of the area of the object to the area in the bounding box is more than 0.9 are removed.

#### 6 | POSTPROCESSING TO REMOVE NOISE

The hair mask at this stage contains false positive objects caused by narrow, hair-like objects, which include pigment network lines and bubbles. False nonhair objects have geometric, location, and color characteristics that distinguish them from hairs. We calculated geometric, color, and location characteristics for all objects detected as hairs for the 707 lesions in the postprocessing training set.

Many false positive objects are pigment network lines within the lesion borders. To detect the false positive objects, we first break the predicted hair segments by skeletonizing all hair candidates and breaking the mask at all branch points. This effectively broke the identified hair segments into smaller segments. Each of the smaller segments is classified as either a true positive or a false positive hair object using a random forest classifier.<sup>28</sup> The false positive objects were removed from the segmented hair mask. Finally, we performed a binary closing operation with a  $5 \times 5$  structuring element to close the gaps between the remaining filtered hair objects, improving recall. The classifier labeled objects with high eccentricity as hair and other objects with high red variance, location within the lesion, and small object size (Figure 8) as a falsely identified hair segment. Postprocessing resulted in an improvement of precision from 0.54 to 0.57, recall from 0.56 to 0.59, dice similarity coefficient from 0.49 to 0.53, and Jaccard from 0.35 to 0.38.

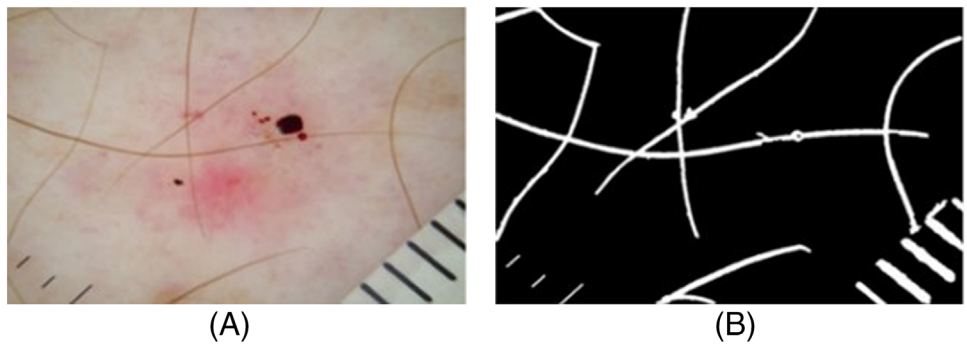


**FIGURE 7** The resultant mask, a logical OR operation between the hair mask and ruler marks.

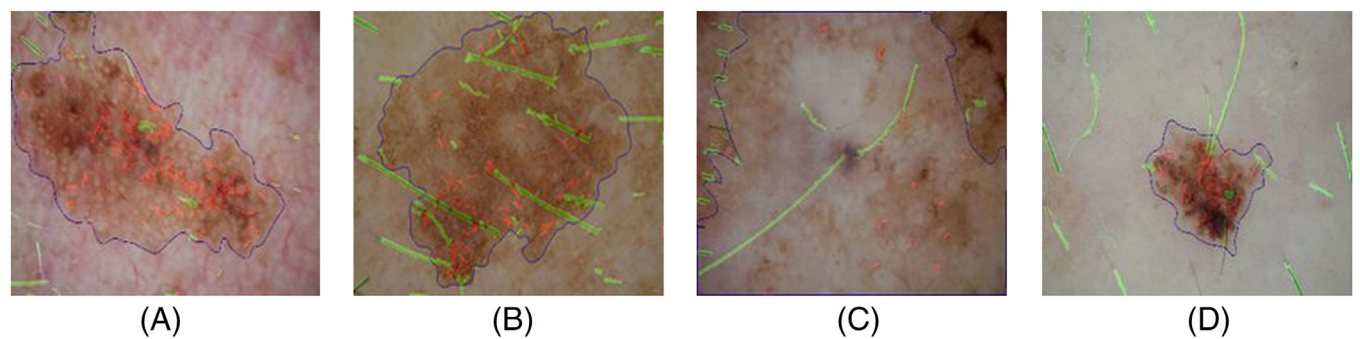


**FIGURE 8** Final results. Four lesions in (A–D) with final hair-ruler mask classifier decisions: red: objects removed, green: objects remain. Note false decisions at upper left, two ruler marks missed, and lower left, bubble outline remains. Most pigment network objects are correctly removed.

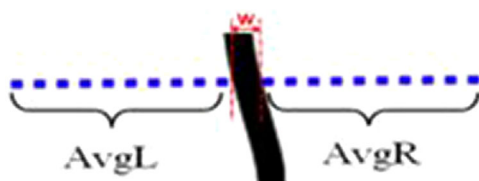


**FIGURE 9** The first step of the inpainting algorithm.

Table 1 shows 18 features and their importance values to detect false positive objects. Both object-level and image-level features are used for the classifier. All but two features are computed on the object-level except for the total number of broken objects in the mask and Y-coordinate of lesion centroid, computed at the image-level.

## 7 | HAIR INPAINTING

The inpainting process is performed in two directions, horizontal and vertical on the R, G and, B planes separately. Hair removal and inpainting results are shown in Figure 9. The inpainting algorithm used to repair and reconstruct the original hair-occluded image, guided by the hair mask, is outlined below.

1. The final hair mask is dilated by a disk of radius 1.

2. For each line of the plane, the averages of the 10 nearby non-hair pixels are computed from the right and the left of the hair,  $\text{AvgR}$ , and  $\text{AvgL}$ , respectively, Figure 10.
3. Construct a vector  $V$ , whose values are computed as the nearest integer to the values for  $V$  calculated as (Equations 9 and 10):
4. Replace the hair pixels in a given line by the vector  $V$ .
5. The resultant image is smoothed, only on the hair edges, by a median filter  $11 \times 11$  window.

$$V = \begin{cases} [\text{AvgR}, \text{AvgR} - (S), \text{AvgR} - (2S), \dots, \text{AvgL}]; & \text{AvgR} > \text{AvgL} \\ [\text{AvgR}, \text{AvgR} + (S), \text{AvgR} + (2S), \dots, \text{AvgL}]; & \text{otherwise} \end{cases} \quad (9)$$

Where  $W$  is the hair width at a given line (Figure 10), and

$$S = \frac{(\text{AvgR} - \text{AvgL})}{(W - 1)} \quad (10)$$

## 8 | RESULTS AND DISCUSSION

### 8.1 | Experimental results

The proposed SharpRazor algorithm with postprocessing to remove noise is trained on 520 dermoscopic images including melanoma, basal cell carcinoma, and benign skin lesions obtained from the studies

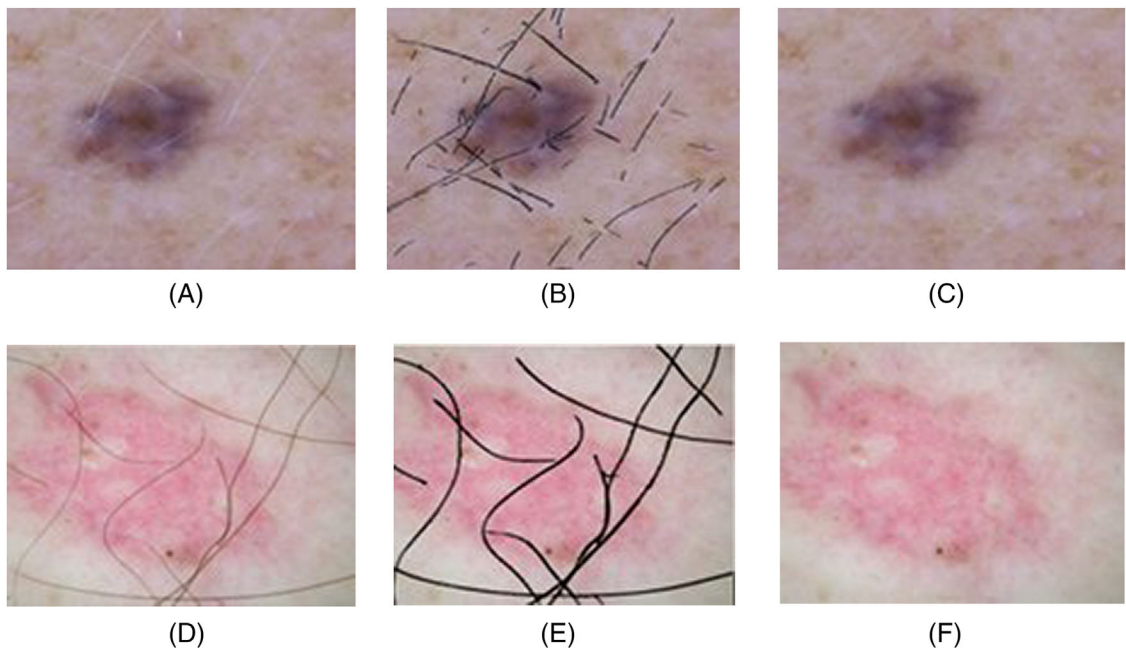


**FIGURE 10** White and dark hair detection and image inpainting. (A) White hair original image. (B) White hair mask. (C) White hair image inpainted. (D) Dark hair original image. (E) Dark hair mask. (F) Dark hair image inpainted.

**TABLE 1** Feature importance values of FP removal classifier

Feature details	Importance value
Total number of broken objects in mask	0.180
Mean color of B-plane in LAB space	0.130
Standard deviation color of R-plane in RGB space	0.090
Eccentricity	0.085
Standard deviation color of B-plane in RGB space	0.080
Average width	0.075
Mean color of A-plane in LAB space	0.055
Object inside lesion	0.055
Standard deviation color of A-plane in LAB space	0.050
Mean color of third plane (PCT)	0.040
Mean color of second plane (PCT)	0.035
Lesion area	0.030
Distance from peak color A-plane in LAB space of nonlesion region	0.025
Euclidean distance from center	0.020
Major axis length	0.015
Extent	0.015
Y-coordinate of lesion centroid	0.015
Y-coordinate of centroid	0.005

R43 CA153927-01 and CA101639-02A2. Postprocessing to remove noise and improve accuracy is trained on 707 lesions from the same dataset. The second dataset for testing includes dermoscopic images and manual masks from Lee et al.<sup>17</sup>

The following metrics are computed for SharpRazor and the seven comparison algorithms.<sup>10,12–14,17,18,24</sup>

$$\text{Accuracy} = \frac{\text{TP} + \text{TN}}{\text{TP} + \text{FP} + \text{FN} + \text{TN}} \quad (11)$$

$$\text{Inaccuracy} = \frac{\text{FP}}{\text{FP} + \text{TN}} + \frac{\text{FN}}{\text{FN} + \text{TP}} \quad (12)$$

$$\text{Precision} = \frac{\text{TP}}{\text{TP} + \text{FP}} \quad (13)$$

$$\text{Recall} = \frac{\text{TP}}{\text{TP} + \text{FN}} \quad (14)$$

$$\text{DSC} = \frac{2\text{TP}}{2\text{TP} + \text{FP} + \text{FN}} \quad (15)$$

$$\text{JAC} = \frac{\text{TP}}{\text{TP} + \text{FP} + \text{FN}} \quad (16)$$

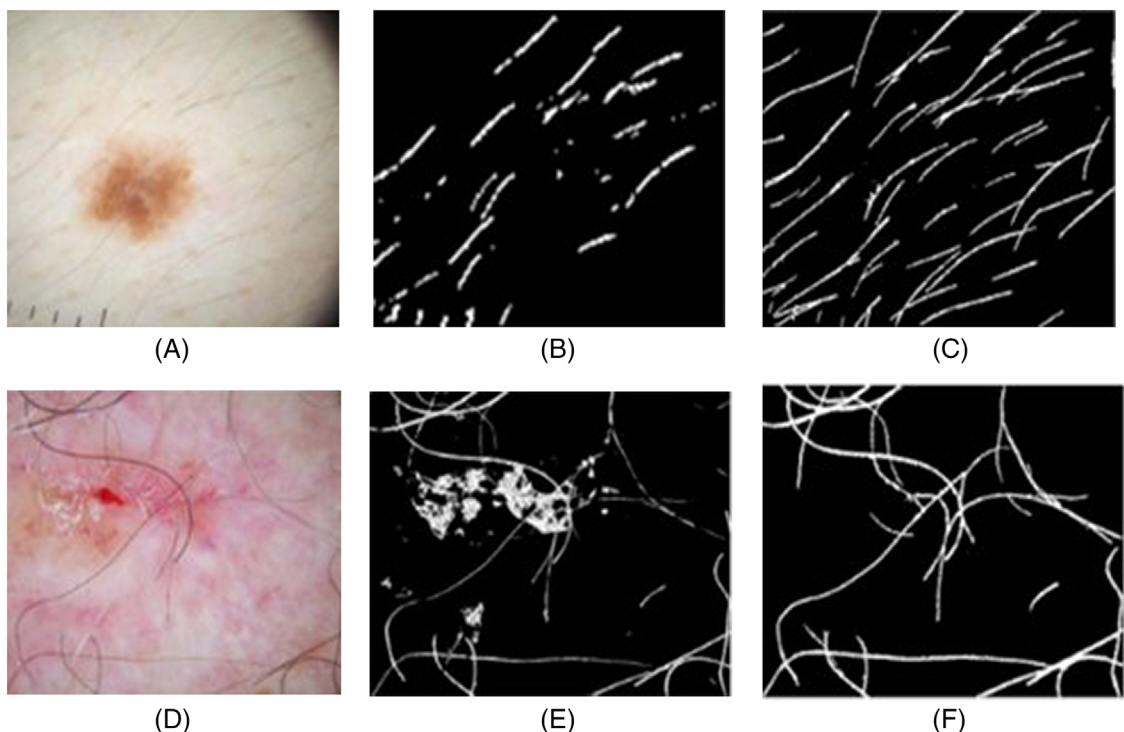
The performance of all eight techniques is shown in Table 2. Most of the SharpRazor improvements are due to better detection of fine hair. Noise immunity is gained by eliminating false hair objects in post-processing. The ability of SharpRazor to detect thin or white-colored hair is shown in Figure 11. Figure 12 provides a visual comparison of the SharpRazor results with the alternative methods listed in Table 2.

## 8.2 | Lesions covered with hair

The proposed algorithm performs well on lesions in areas such as the scalp covered with hair, where lesion segmentation algorithms often

**TABLE 2** SharpRazor results compared with seven existing hair segmentation algorithms on 25 test images

	Acc	Inacc	Prec	Rec	Dsc	Jac
SharpRazor, 2021	93.76	22.32	0.57	0.59	0.53	0.38
Ian Lee, 2017	90.99	29.39	0.60	0.44	0.40	0.26
Xie, 2015	90.04	39.07	0.37	0.25	0.25	0.15
Koehoorn, 2015	80.13	49.11	0.08	0.14	0.07	0.03
Abbas, 2013	87.36	29.40	0.34	0.49	0.33	0.22
Huang, 2013	19.02	66.82	0.05	0.50	0.08	0.04
Fiorese, 2011	91.74	37.82	0.68	0.26	0.32	0.20
DullRazor, 1997	93.15	34.87	0.66	0.31	0.38	0.25

**FIGURE 11** Comparison result on images with thin hair (top) and noise (bottom): (A) Original image 1. (B) DullRazor image 1. (C) SharpRazor image 1. (D) Original image 2. (E) DullRazor image 2. (F) SharpRazor image 2.

fail to detect the lesion. Figure 13 shows the result of the proposed algorithm on lesions covered with hair. Inpainting on these lesions is generally imperfect (Figure 14).

### 8.3 | Skin lesion segmentation after hair removal

Hair can interfere with skin lesion segmentation. Figure 13 shows the segmentation of two lesions<sup>29</sup> covered with hair before and after using the proposed hair removal. Using manual segmentation masks, the XOR error of images covered with hair is 33.52% and 53.52% for the first and second lesion, respectively. After removing hair using

SharpRazor, XOR errors fall to 5.83% and 11.25% for the first and second lesion, respectively.

### 8.4 | Limitations

Limitations in the proposed technique are apparent in hairs with low contrast with the skin. Hair may appear so close to skin tones that SharpRazor cannot detect the grayscale difference between hair and background. Precision is lower than some previous methods (Table 2, overall accuracy metrics are higher). An adaptive local threshold could be a solution to overcome these limitations. Manual borders

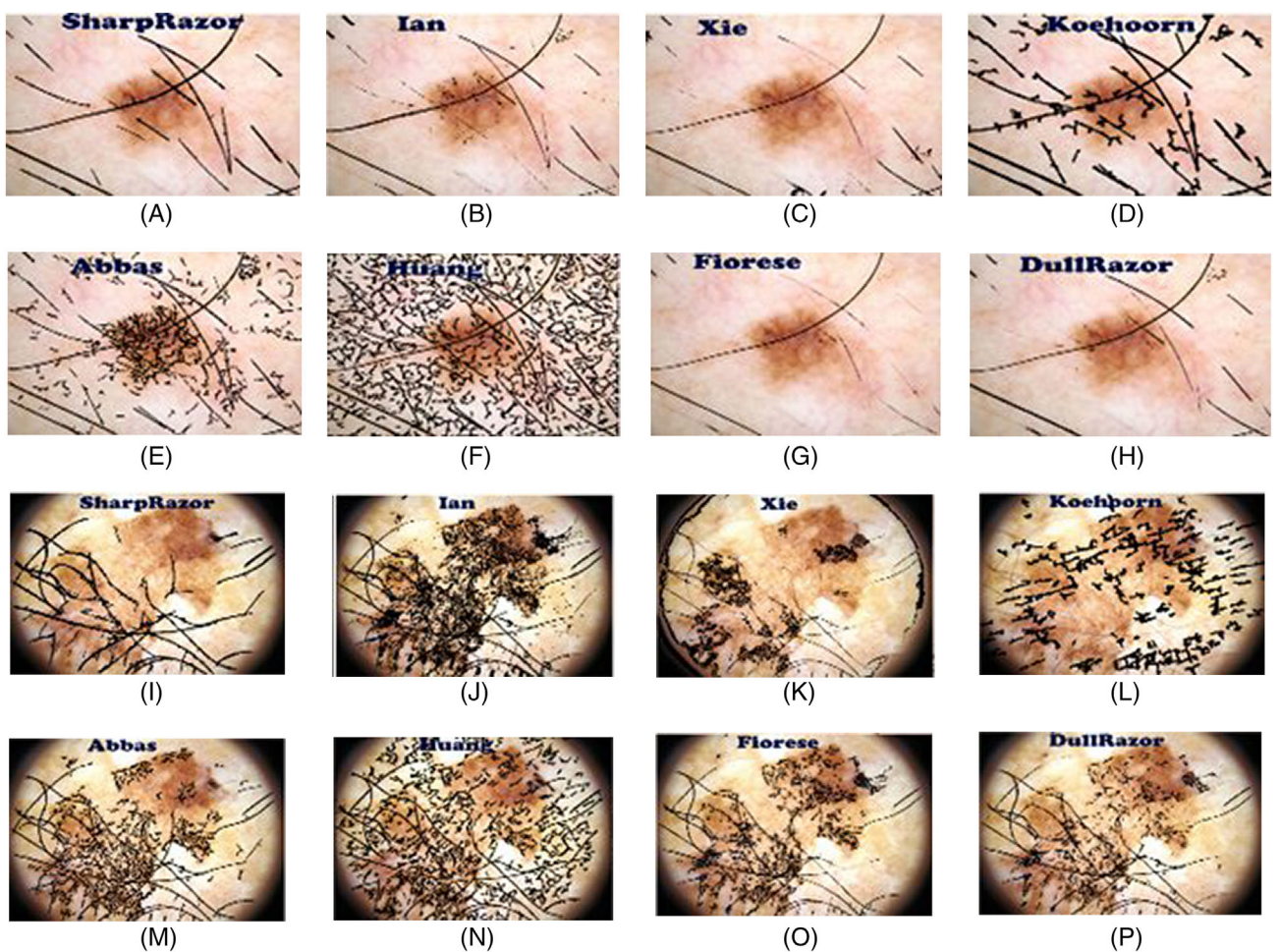


**FIGURE 12** Hair masks overlaid on the original images for eight hair detection methods. (A–H) Image 1 with different hair detection methods. (I–P) Image 2 with different hair detection methods.

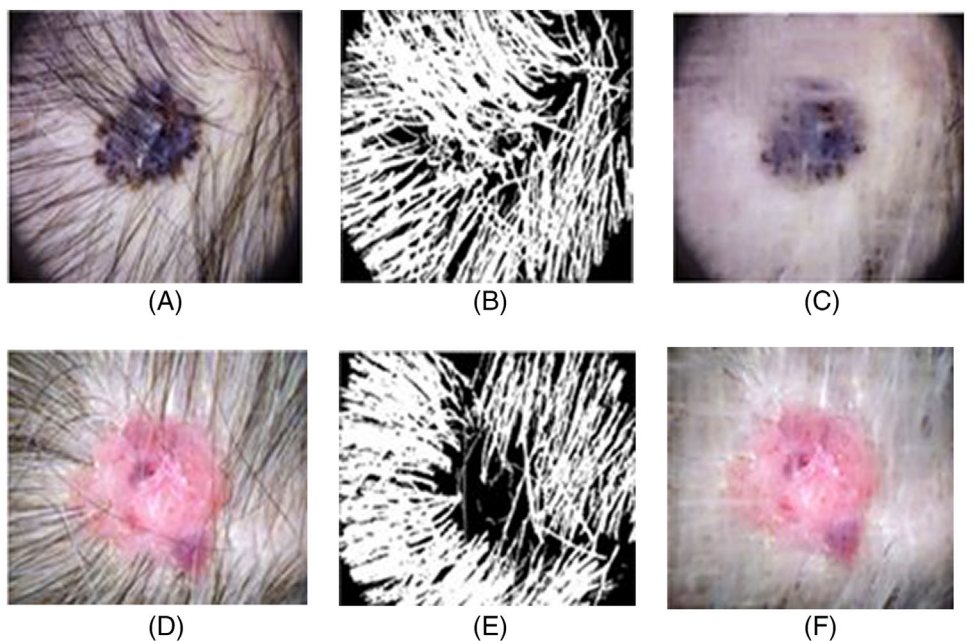


**FIGURE 13** SharpRazor hair removal on lesions covered with hair. (A) Original image 1. (B) Hair mask image 1. (C) Image 1 inpainted. (D) Original image 2. (E) Hair mask image 2. (F) Image 2 inpainted.

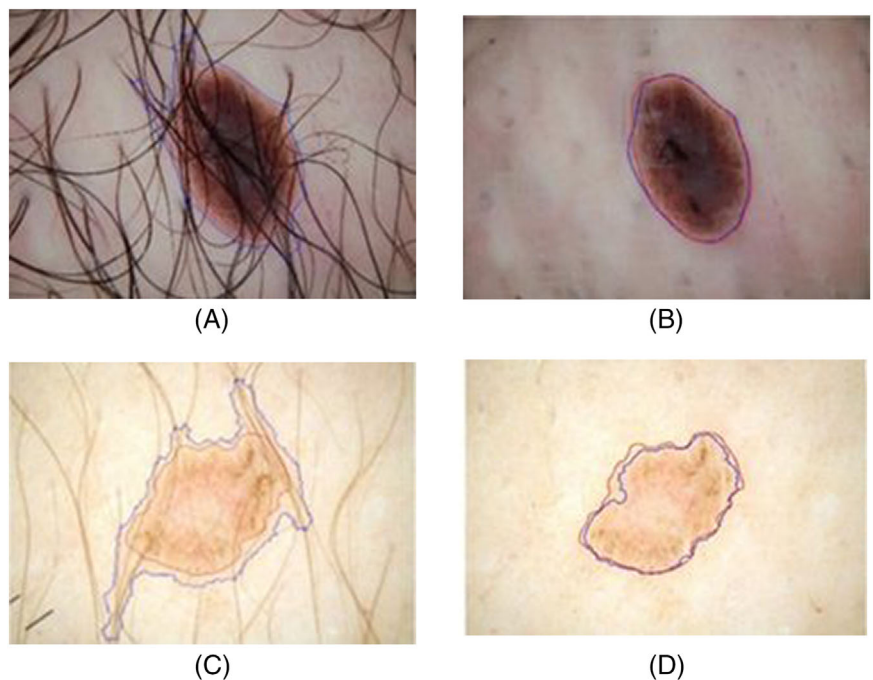


**FIGURE 14** Lesion segmentation examples before and after Sharprazor. (A) Original image 1 segmentation (Error = 33.52%). (B) Image 1 after Sharprazor segmentation (Error = 5.83%). (C) Original image 2 segmentation (Error 53.52%). (B) Image 2 after Sharprazor segmentation (Error = 11.25%).

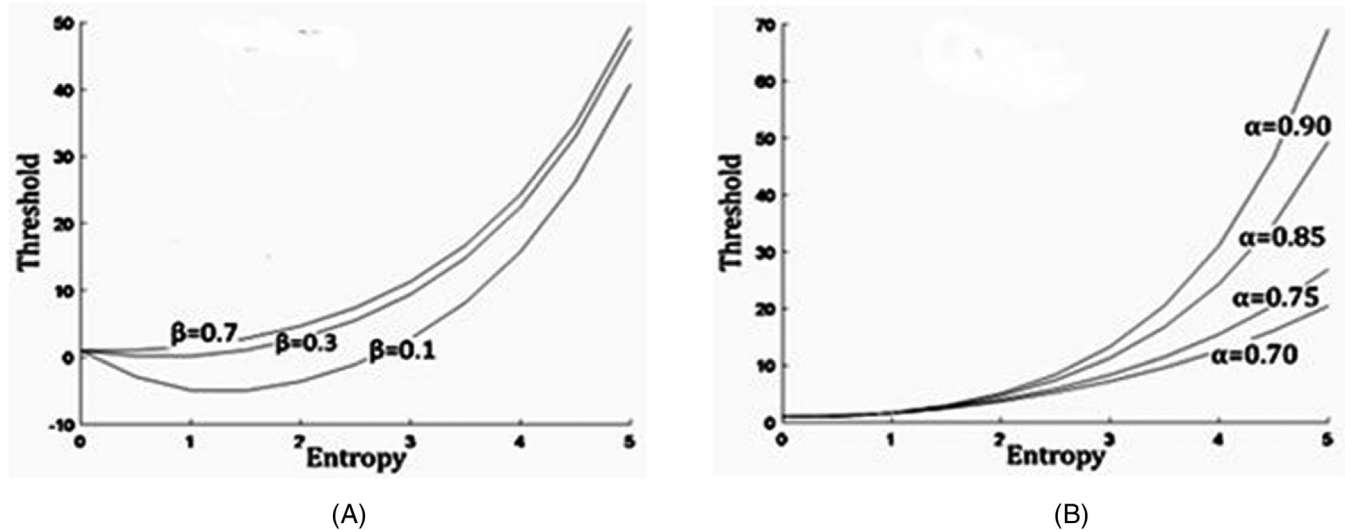


**FIGURE 15** Thresholds controlled by  $\beta$  and  $\alpha$  constants. (A)  $\alpha = 0.85$ . (B)  $\beta = 0.7$ .

trained the borders for the postprocessing noise removal algorithm. The proposed algorithm has not been evaluated on a large, publicly available dataset.

## 9 | CONCLUSION

This paper presents a filter-based technique to remove light and dark hairs and ruler marks in dermoscopic images. The hair removal algorithm includes two filters, each with three panels, which filter images in the horizontal and vertical directions. The triple-panel design enables

the detection of most hairs and ruler marks encountered in these images. The filters obtain a rough estimate for hair structures; hair is segmented using gradients in different orientations then refined. Ruler marks and white hair are detected separately and added to the hair mask. A classifier improves the detection precision and recall at a small cost in recall. Finally, the images are inpainted using a vector-based method.

The basic hair removal algorithm was trained on 520 dermoscopic images, and the postprocessing classifier was trained on 707 images. The final algorithm was tested on 25 images for comparison to seven published methods. Statistical analysis to score the approach used

manual hair masks as ground truth. The proposed SharpRazor algorithm shows state-of-the-art results. It can detect and inpaint both dark and white hair in a wide variety of lesions.

## 10 | APPENDIX—ENTROPY-BASED SEGMENTATION

We developed the following algorithm to provide more adaptable final hair segmentation. The enhanced hair mask is divided into blocks of  $60 \times 60$ . The entropy of each block is used to compute a local threshold  $T$  as Equation 17:

$$T = e^{E^\alpha} - \frac{\tan H(E)}{\beta} \quad (17)$$

E: Entropy (Block based)

e: Exponential

$\tan H$ : Hyperbolic tangent

$\alpha$  : Constant that controls the threshold for large entropy. Large entropies indicate many hairs.

$\beta$ : Constant that controls the threshold for small entropies. Small entropies indicate few hairs.

Figure 15 shows how the two constants affect the thresholding algorithm. In this work, the enhanced hair mask is optimally binarized by choosing  $\beta = 0.7$  and  $\alpha = 0.85$ . After binarization of all the blocks, all objects with area less than 10 and all objects with major axis less than 10 are considered as noise and removed. We applied this algorithm and found minimal change compared to the segmentation algorithm in Section 3; however, it may improve results on other datasets, especially on lesions covered with hair.

## DATA AVAILABILITY STATEMENT

The data that support the findings of this study are available upon request from the corresponding author. The data are not publicly available due to privacy or ethical restrictions.

## REFERENCES

1. Siegel RL, Miller KD, Fuchs HE, Jemal A. Cancer statistics. *CA Cancer J Clin.* 2021;71(1):7-33.
2. Rogers HW, Weinstock MA, Feldman SR, Coldiron BM. Incidence estimate of nonmelanoma skin cancer (keratinocyte carcinomas) in the US population. 2012. *JAMA Dermatol.* 2015;151(10):1081-1086.
3. Bray F, Ferlay J, Soerjomataram I, Siegel RL, Torre LA, Jemal A. Global cancer statistics 2018: GLOBOCAN estimates of incidence and mortality worldwide for 36 cancers in 185 countries. *CA Cancer J Clin.* 2018;68(6):394-424.
4. Esteve A, Kuprel B, Novoa RA, et al. Dermatologist-level classification of skin cancer with deep neural networks. *Nature.* 2017;542(7639):115-118.
5. Tschandl P, Codella N, Akay BN, et al. Comparison of the accuracy of human readers versus machine-learning algorithms for pigmented skin lesion classification: an open, web-based, international, diagnostic study. *Lancet Oncol.* 2019;20(7):938-947.
6. Ferris LK, Harkes JA, Gilbert B, et al. Computer-aided classification of melanocytic lesions using dermoscopic images. *J Am Acad Dermatol.* 2015;73(5):769-776.
7. Haenssle HA, Fink C, Schneiderbauer R, et al. Man against machine: diagnostic performance of a deep learning convolutional neural network for dermoscopic melanoma recognition in comparison to 58 dermatologists. *Ann Oncol.* 2018;29(8):1836-1842.
8. Hagerty JR, Stanley RJ, Almubarak HA, et al. Deep learning and handcrafted method fusion: higher diagnostic accuracy for melanoma dermoscopy images. *IEEE J Biomed Health Inform.* 2019;23(4):1385-1391.
9. Barata C, Celebi ME, Marques JS. A survey of feature extraction in dermoscopy image analysis of skin cancer. *IEEE J Biomed Health Inform.* 2018;23(3):1096-1109.
10. Fiorese M, Peserico E, Silletti A. VirtualShave: automated hair removal from digital dermatoscopic images. Paper presented at: 2011 Annual International Conference of the IEEE Engineering in Medicine and Biology Society; August 30-September 03, 2011; Boston, MA, USA.
11. Abbas Q, Celebi M, García I. Hair removal methods: a comparative study for dermoscopy images. *Biomed Signal Process Control.* 2011;6(4):395-404. <https://doi.org/10.1016/j.bspc.2011.01.003>
12. Lee I, Du X, Anthony B. Hair segmentation using adaptive threshold from edge and branch length measures. *Comput Biol Med.* 2017;89:314-324.
13. Xie F-Y, Qin S-Y, Jiang Z-G, Meng R-S. PDE-based unsupervised repair of hair-occluded information in dermoscopy images of melanoma. *Comput Med Imaging Graph.* 2009;33(4):275-282.
14. Abbas Q, Garcia IF, Emre Celebi M, Ahmad W. A feature-preserving hair removal algorithm for dermoscopy images. *Skin Res Technol.* 2013;19(1):e27-e36.
15. Bornemann F, März T. Fast image inpainting based on coherence transport. *J Math Imaging Vision.* 2007;28(3):259-278.
16. Nguyen NH, Lee TK, Atkins MS. Segmentation of light and dark hair in dermoscopic images: a hybrid approach using a universal kernel. Paper presented at: Medical Imaging 2010: Image Processing; March 12, 2010; San Diego, CA.
17. Lee T, Ng V, Gallagher R, Coldman A, McLean D. Dullrazor®: a software approach to hair removal from images. *Comput Biol Med.* 1997;27(6):533-543.
18. Koehoorn J, Sobiecki AC, Boda D, et al. Automated digital hair removal by threshold decomposition and morphological analysis. *International Symposium on Mathematical Morphology and Its Applications to Signal and Image Processing.* Springer; 2015.
19. Toossi MTB, Pourreza HR, Zare H, Sigari MH, Layegh P, Azimi A. An effective hair removal algorithm for dermoscopy images. *Skin Res Technol.* 2013;19(3):230-235.
20. Kiani K, Sharafat AR. E-shaver: an improved DullRazor® for digitally removing dark and light-colored hairs in dermoscopic images. *Comput Biol Med.* 2011;41(3):139-145.
21. Fleming MG, Steger C, Zhang J, Gao J, Cognetta AB, Dyer CR. Techniques for a structural analysis of dermatoscopic imagery. *Comput Med Imaging Graph.* 1998;22(5):375-389.
22. Steger C. An unbiased detector of curvilinear structures. *IEEE Trans Pattern Anal Mach Intell.* 1998;20(2):113-125.
23. Abuzaghleh O, Barkana BD, Faezipour M. Noninvasive real-time automated skin lesion analysis system for melanoma early detection and prevention. *IEEE J Trans Eng Health Med.* 2015;3:1-12.
24. Huang A, Kwan S-Y, Chang W-Y, Liu M-Y, Chi M-H, Chen G-S. A robust hair segmentation and removal approach for clinical images of skin lesions. Paper presented at: 2013 35th Annual International Conference of the IEEE Engineering in Medicine and Biology Society (EMBC). July 03-07, 2013; Osaka, Japan.
25. Zhou H, Chen M, Gass R, et al. Feature-preserving artifact removal from dermoscopy images. Paper presented at: Medical Imaging 2008: Image Processing. March 27, 2008; San Diego, CA.

26. Itoh K, Ohno Y. A curve fitting algorithm for character fonts. *Electronic publishing*. 1993;6(3):195-205.
27. Otsu N. A threshold selection method from gray-level histograms. *IEEE Trans Syst Man Cybern*. 1979;9(1):62-66.
28. Hastie T, Tibshirani R, Friedman J. *Random forests. The Elements of Statistical Learning*. Springer; 2009.
29. Tschandl P, Rosendahl C, Kittler H. The HAM10000 dataset, a large collection of multi-source dermatoscopic images of common pigmented skin lesions. *Sci Data*. 2018;5(1):1-9.

**How to cite this article:** Kasmi R, Hagerty J, Young R, et al.

SharpRazor: Automatic removal of hair and ruler marks from dermoscopy images. *Skin Res Technol*. 2023;29:e13203.

<https://doi.org/10.1111/srt.13203>